Tropical Impacts of SST Forcing: A Case Study for 1987 versus 1988

LEONARD M. DRUYAN

NASA/Goddard Institute for Space Studies and Columbia University, New York, New York

STEFAN HASTENRATH

Department of Atmospheric and Oceanic Sciences, University of Wisconsin–Madison, Madison, Wisconsin

(Manuscript received 6 July 1993, in final form 30 November 1993)

ABSTRACT

The response of the NASA/Goddard Institute for Space Studies GCM to large tropical sea surface temperature (SST) anomalies is investigated by evaluating model simulations of the particularly contrasting summer monsoon seasons 1987 and 1988. These years are representative of the warm and cold phases, respectively, of a recent ENSO event. An ensemble averaging the results of three simulations was considered for each season, using monthly mean observed SST anomalies for June–August 1987 and 1988 as lower boundary forcing. Consistent with the ECMWF-analyzed winds, the simulations based on 1988 as compared to 1987 SST exhibit stronger upper-tropospheric irrotational circulation between the monsoon regions and the Southern Hemispheric subtropical anticyclones, a stronger Pacific Walker cell and a weaker subtropical westerly jet over the South Pacific. In the same vein, the modeled precipitation, indicating a more northerly position of the Pacific ITCZ in 1988 compared with 1987, is supported by satellite observations of outgoing longwave radiation and highly reflective clouds.

1. Introduction

This research grew out of a workshop of the Monsoon Numerical Experimentation Group (MONEG) held at the National Center for Atmospheric Research, Boulder, Colorado, in October 1991. The focus of the workshop was a discussion of results from experimentation coordinated among 16 climate modeling groups. Each of their general circulation models (GCMs) was used to simulate two particular summer monsoon seasons, 1987 and 1988, using the corresponding globally observed sea surface temperature (SST) as lower boundary forcing (Figs. 1a and 1b). These particular seasons represent opposite extremes in monsoon activity, 1987 being considerably drier than 1988 over India and the Sahel. In addition, a Pacific El Niño event was in its warm phase during the summer of 1987, but had already developed large cold anomalies by the following summer. The extreme SST differences in the Pacific Ocean can be seen in Fig. 1c. Results of these experiments are described in the report of the workshop (World Meteorological Organization 1992) and subsequent journal publications (Palmer et al. 1992; Mo 1992). The present paper discusses the results from simulations with the Goddard Institute for Space Studies (GISS) GCM (model II, Hansen et al. 1983).

Corresponding author address: Leonard M. Druyan, NASA/Goddard Institute for Space Studies, Columbia University, 2880 Broadway, New York, NY 10025.

2. Experimental design

Motivated by the contrasting climate anomalies of 1987 and 1988, GISS model simulations were made with observed SST from those years used as boundary forcing. For the purpose of these simulations, Reynolds's (1988) analyses of monthly mean SST in the global domain formed the basis for interpolation to daily SST values between 1 June and 30 August. National Meteorological Center (NMC) initial atmospheric conditions at 0000 UTC on 1, 2, and 3 June 1987 and 1988 were interpolated to the three-dimensional model grid to initialize the six simulations.

The version of the GCM used in the present study has a horizontal resolution of 4° latitude by 5° longitude and nine levels in the vertical. Each grid element is divided into land and ocean fractions, and two ground layers are used for surface hydrology calculations that keep track of heat and ground moisture storage. Physical processes contained in the model include solar and terrestrial radiation transfer and their interaction with computed clouds. Vertical transports of moisture, heat, and momentum are accomplished by convection. The GISS model II uses a simple mass flux cumulus parameterization, which is fully described by Del Genio and Yao (1993). Moist convection is diagnosed to occur whenever a parcel of air lifted adiabatically from some level is buoyant with respect to the environment at the next higher level, the parcel rising to the highest consecutive level at which the

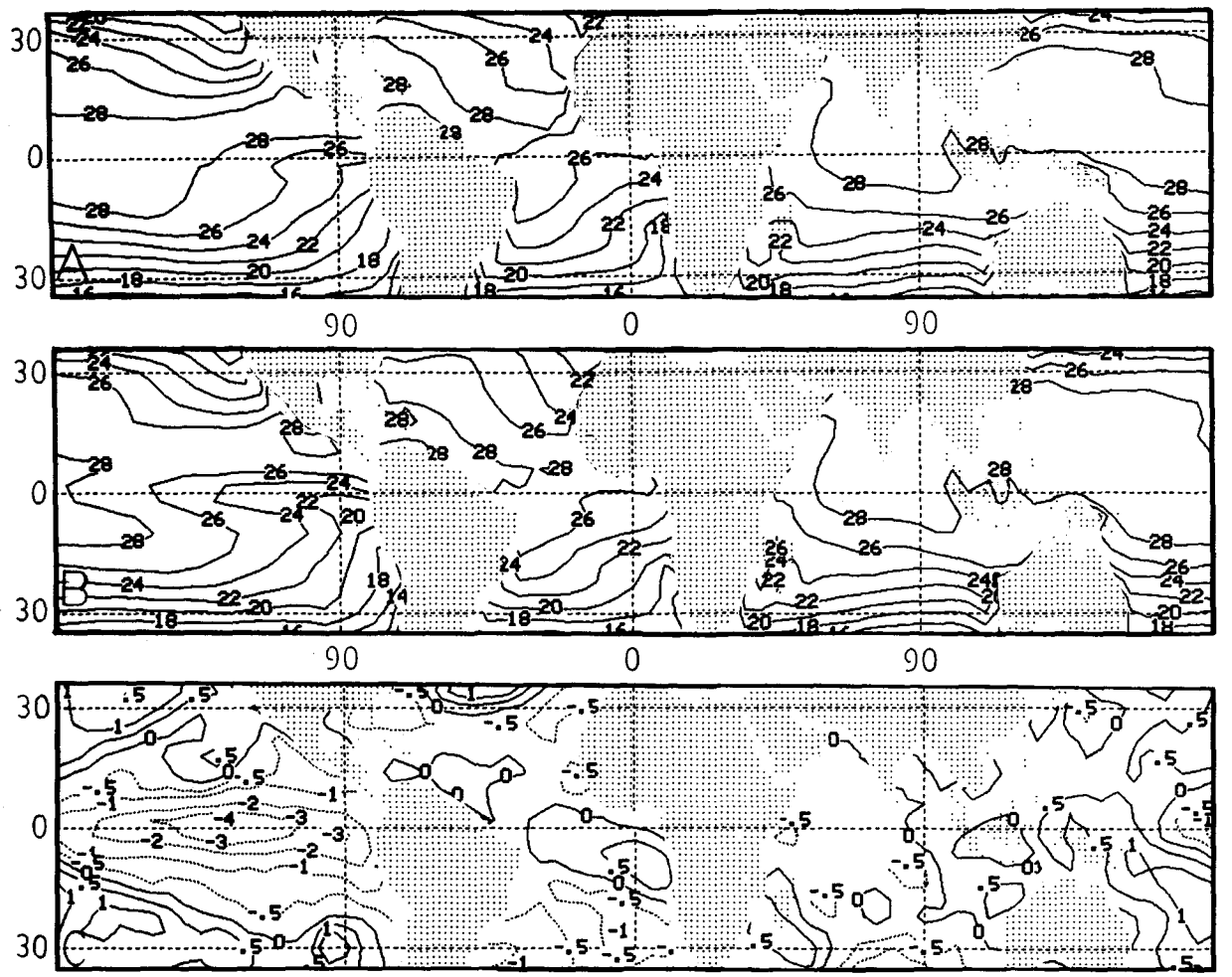

FIG. 1. Sea surface temperature (°C) for June–August: (a) 1987, (b) 1988, and (c) 1988 minus 1987.

buoyancy criterion is satisfied. A fixed 50% of the mass of the cloud-base layer rises in each event, without any additional entrainment into the rising plume. Heating of the environment results from compensating subsidence, cooling from reevaporation of falling precipitation.

We refer to the ensemble average of the three simulations using 1987 SST as ENS87, and the ensemble average of the three simulations based on 1988 SST as ENS88. Comparison of ensemble results increases the signal-to-noise ratio, giving a more accurate estimate of the impact of SST forcing on simulated variables.

3. Observations

a. Global winds

June–August mean wind components at 200 mb from the ECMWF dataset with 2° × 2° resolution were analyzed on the GISS GCM 4° × 5° resolution grid. The resulting fields of velocity potential are displayed in Figs. 2a–c, while the corresponding streamfunction patterns are mapped in Figs. 3a–c. These observed fields serve as a reference for the model results that are discussed in section 4. For a discussion of the observed upper-tropospheric patterns during the boreal summers of 1987 and 1988, refer to Krishnamurti et al. (1989, 1990), Palmer et al. (1992), and Mo (1992).

b. Convective clouds

Figures 4a and 4b map the observed June–August patterns of outgoing longwave radiation (OLR) for 1987 and 1988, and Fig. 4c shows the 1988 minus 1987 differences. Similarly, Figs. 5a and 5b depict the distribution of highly reflective clouds (HRC) for 1987 and 1988, and Fig. 5c shows the 1988 minus 1987 differences. In conjunction, the OLR and HRC maps indicate that the ITCZ over the Pacific Ocean was located farther north in June–August 1988 than in 1987. In particular, the HRC maximum over the eastern Pacific was at 8°–10°N in 1987 but at about 12°N in

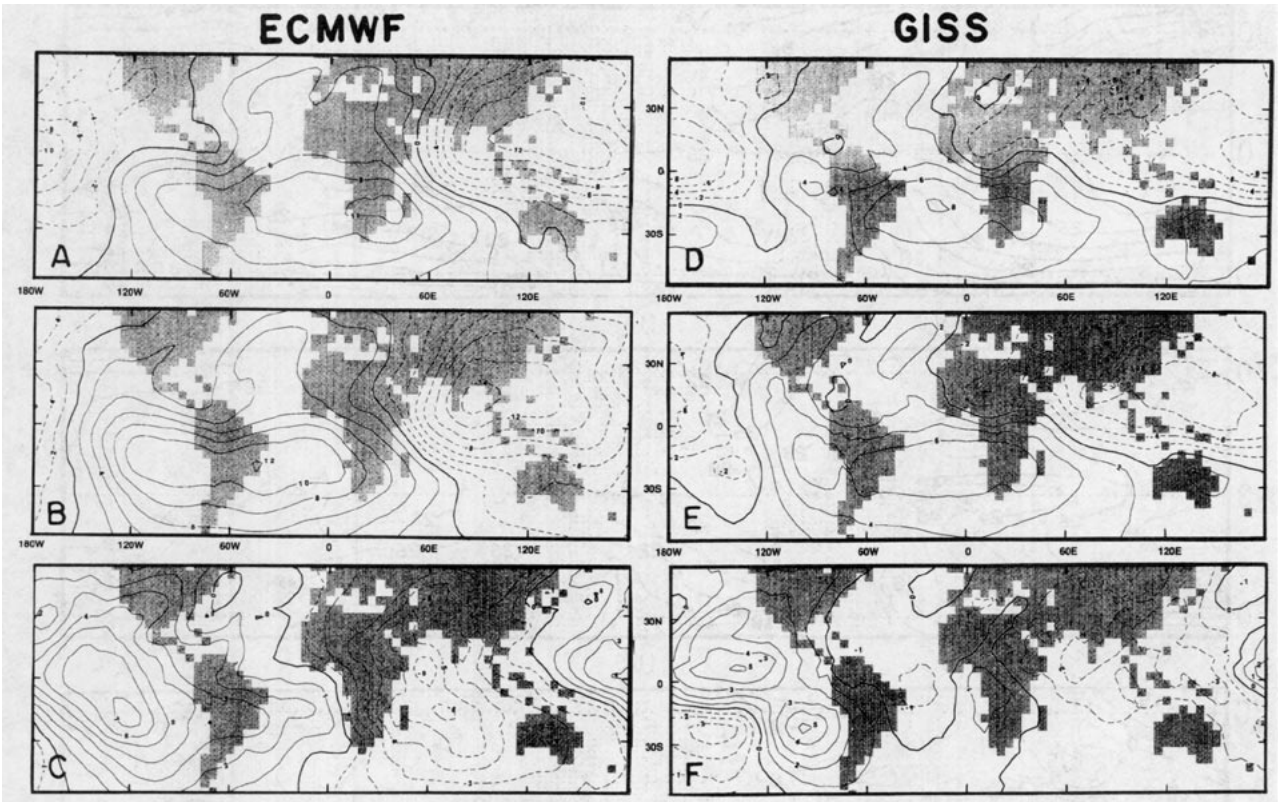

FIG. 2. Velocity potential of June–August 200-mb winds: (a) ECMWF 1987; (b) ECMWF 1988; (c) ECMWF, 1988 minus 1987; (d) run ENS87; (e) run ENS88; (f) ENS88 minus ENS87. Isopleth spacing is 2×10^6 m^2 s^{-1} for (a), (b), (c), (d), and (e), but 1×10^6 m^2 s^{-1} for (c) and (f); broken lines indicate negative values.

1988. Similarly, the OLR minimum in 1988 was at 10°–12°N over the eastern Pacific compared with its 1987 position at 5°–8°N. Both the OLR and HRC difference maps (Figs. 4c and 5c) imply a more northerly location of the band of organized convection in June–August 1988 as compared to 1987.

Station observations of precipitation over the Sahel and over India indicate a somewhat rainier season in 1988 (Arkin 1992). This is consistent with positive 1988 minus 1987 differences in HRC frequency for both locations (Fig. 5c). OLR differences sustain this assessment, but they may not be a good proxy for rainfall over West Africa (Arkin 1992).

4. Modeled global-scale wind fields

Model level seven is a surface of constant sigma, the vertical coordinate used in the GISS model. Atmospheric pressure along this surface is approximately 200 mb at most grid elements, so the circulation at this level can reasonably be compared to observed wind fields constructed for the 200-mb constant pressure surface (Figs. 2a–c and 3a–c). Figures 2d and 2e show the model level seven (hereafter 200 mb) velocity potential averaged for June–August from the simulation ensembles based on 1987 and 1988 SST (ENS87 and ENS88), and Fig. 2f maps the ENS88 minus ENS87 difference field. The modeled distributions for both seasons capture the general features of the observed dipole pattern (Figs. 2a and 2b). Each includes a center of negative values over the western Pacific Ocean and southern Asia, indicating the location of upper-tropospheric outflow over the summer monsoon region, in juxtaposition to a positive area across the South Atlantic and the eastern South Pacific that traces the axis of convergence aloft over the subtropical anticyclones and over the subsiding portion of the Pacific Walker cell. The pattern over the Himalayas is somewhat noisy, as are most of the model's wind and geopotential height fields in this region, presumably due to mountain-induced perturbations.

The model's depiction of a slightly stronger minimum of 200-mb velocity potential over India and of the outflow above the monsoon area in 1988 as compared to 1987 (Figs. 2d and 2e) is supported by observations (Figs. 2a and 2b). In this respect, the model circulation has responded to the differential SST forcing in the proper sense. However, for both years the simulated outflow over the western North Pacific is too diffuse and extends too far east. These results can be compared to similar experiments with the NMC T80 model of 1990 by Mo (1992), who found that her

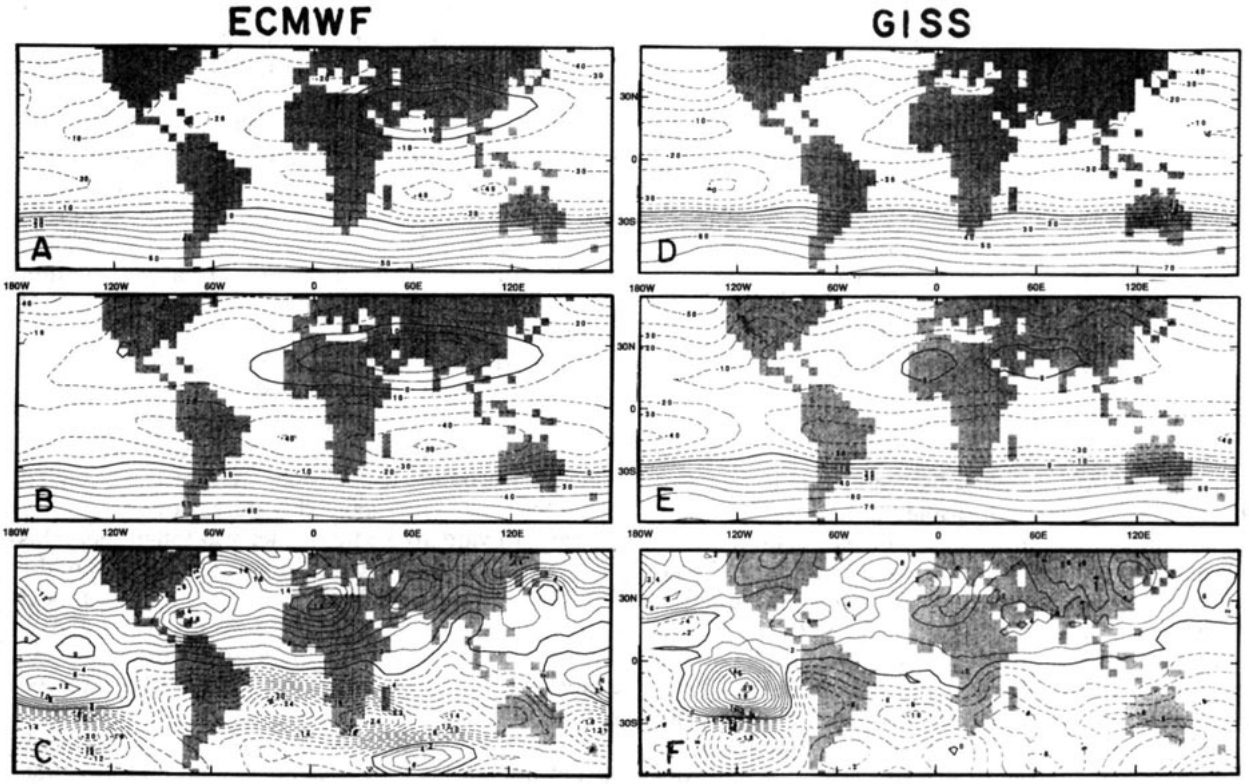

FIG. 3. Streamfunction of June–August 200-mb winds: (a) ECMWF 1987; (b) ECMWF 1988; (c) ECMWF, 1988 minus 1987; (d) run ENS87; (e) run ENS88; (f) ENS88 minus ENS87 (units: 10^6 m^2 s^{-1}). Isopleth spacing is 10×10^6 m^2 s^{-1} for (a), (b), (c), (d), and (e), but 2×10^6 m^2 s^{-1} for (c) and (f); broken lines indicate negative values.

model's response was not sensitive enough to the 1988 minus 1987 differences in SST boundary conditions to alter the position of the velocity potential minimum over the western Pacific. In a parallel study using the ECMWF T42L19 (cycle 34) GCM, very skillful simulations of these interannual differences in velocity potential were made (Palmer et al. 1992).

The modeled divergent circulation is somewhat weaker than observed, based on the less pronounced extrema of the velocity potential (Figs. 2d and 2e compared to Figs. 2a and 2b). There are two centers of outflow indicated by the simulations, and the positions of the more easterly center (180° longitude in ENS87 and 140°E in ENS88) reflect an excess of modeled divergence well to the east of the observed monsoon outflow. A tongue of negative potential extending into the southeast Pacific further implies that the model has allowed significant convection there, narrowing the zonal dimension of the Walker cell. This discrepancy is more pronounced in ENS88.

The large centers of positive and negative ENS88 minus ENS87 differences in velocity potential simulated by the GCM (Fig. 2f) correspond fairly well to the observed pattern (Fig. 2c). The positive values over the eastern Pacific Ocean, indicative of stronger 200-mb convergence in 1988, cover similar areas in the modeled and observed versions. However, the model produced somewhat smaller values and a split into two separate centers, as well as a negative domain in the southwestern corner of the map area; the last feature is the direct consequence of the tongue of negative values in ENS88 (Fig. 2e). The model further shows a center of negative differences over South Asia and the Indian Ocean, representing the stronger divergence above the monsoon convection of 1988.

Comparison of Figs. 2d and 2e reveals little difference between the ENS88 and ENS87 velocity potential

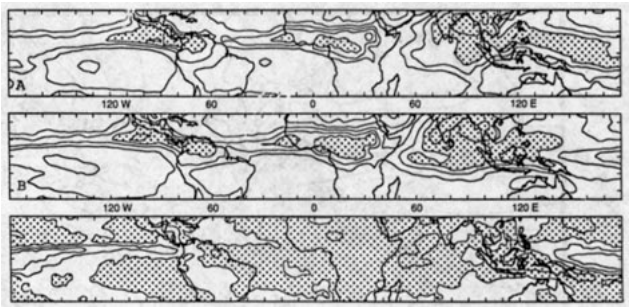

FIG. 4. Outgoing longwave radiation for June–August: (a) 1987, (b) 1988, and (c) ΔOLR, 1988 minus 1987. Contour interval is 20 W m^{-2}; dot raster indicates OLR < 220 W m^{-2} and ΔOLR < 0.

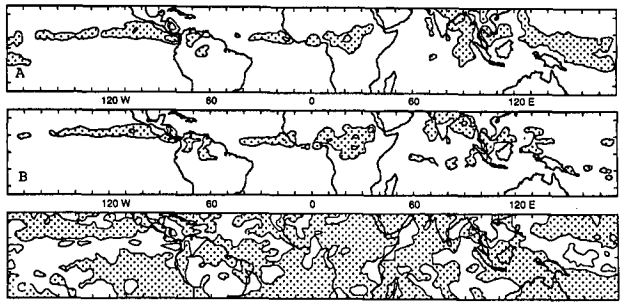

FIG. 5. Highly reflective clouds for June–August: (a) 1987, (b) 1988, and (c) ΔHRC, 1988 minus 1987. Contour interval is 5 days month^{-1}; dot raster indicates HRC > 5 days month^{-1} and ΔHRC < 0.

over tropical Africa. The observations (Figs. 2a and 2b), on the other hand, display a distinctly stronger gradient in 1988, indicative of stronger irrotational circulation associated with the tropical easterly jet (TEJ).

Figures 3d,e show the June–August streamfunction at 200 mb forced by 1987 and 1988 SST, and Fig. 3f depicts the ENS88 minus ENS87 difference field. The gradient over Africa and the Indian Ocean at 0°–20°N reflects the strength of the TEJ. Reference to the observed patterns in Figs. 3a and 3b shows that the modeled TEJ is weaker and displaced southward of its observed position over India and the Indian Ocean for both ensembles. ENS87 gives a realistic representation of the nondivergent circulation over tropical Africa (Fig. 3d compared to Fig. 3a) while the ENS88 streamfunction gradient is too diffuse and does not indicate the stronger easterlies in 1988 over the Sahel (Fig. 3e) apparent from the corresponding ECMWF analysis (Fig. 3b).

The subtropical westerlies over the South Pacific are weaker for ENS88 than ENS87, a well-documented aspect of contrasting phases of the Southern Oscillation (Philander 1990, 33). The streamfunction patterns from ECMWF (Figs. 3a,b) confirm the weaker Southern Hemisphere subtropical westerly jet (SWJ) and the lesser zonal extent of tropical easterlies over the Pacific in 1988, although the latter was not reproduced well by the model. In fact, ENS88 produced a westerly upper portion of the Walker cell confined to a narrow longitudinal interval over the eastern Pacific. A similar deficiency was found in the simulation of June–August 1988 circulation by the NMC T80 spectral model of 1990 (Mo 1992), which maintained 200-mb easterlies over the entire equatorial Pacific, with only a slight weakening near 150°W. In the GISS GCM, the problem may derive from an excess transport of easterly momentum upward from the near-surface circulation by overly vigorous convection (Rind 1993, personal communication).

Modeled differences in the ENS88 minus ENS87 streamfunction at 200 mb are shown in Fig. 3f. One of the more prominent features of this field is the cyclonic gyre over the southeast Pacific at about 15°S, which corresponds to a similar gyre in the observed field (Fig. 3c). The modeled feature, however, is displaced eastward by some 40 degrees longitude. This discrepancy also reflects the limited zonal extent of the modeled mid-Pacific Walker cell in the basic model climatology as well as in ENS88, as discussed above. Additionally, we note that the location of the anticyclonic cell over 35°S corresponds well to the observed pattern.

The ENS88 minus ENS87 differences in 200-mb streamfunction indicate a slightly stronger TEJ in 1988 over northern Africa and over the north Indian Ocean, although the rather weak gradient indicates that these modeled interannual differences (Fig. 3f compared with Fig. 3c) were grossly underestimated. As discussed above, a comparison of Figs. 2a–c and 3a–c with Figs. 2d–f and 3d–f reveals that both the nondivergent and the irrotational components of the 200-mb wind were underestimated over northern Africa in ENS88.

5. Precipitation

Figure 6 shows the five-year mean precipitation rate for June–August from a control run based on long-term mean observed SST. The ITCZ maximum across northern Africa is realistic compared with climatology (Shea 1986), while the gradient toward drier conditions

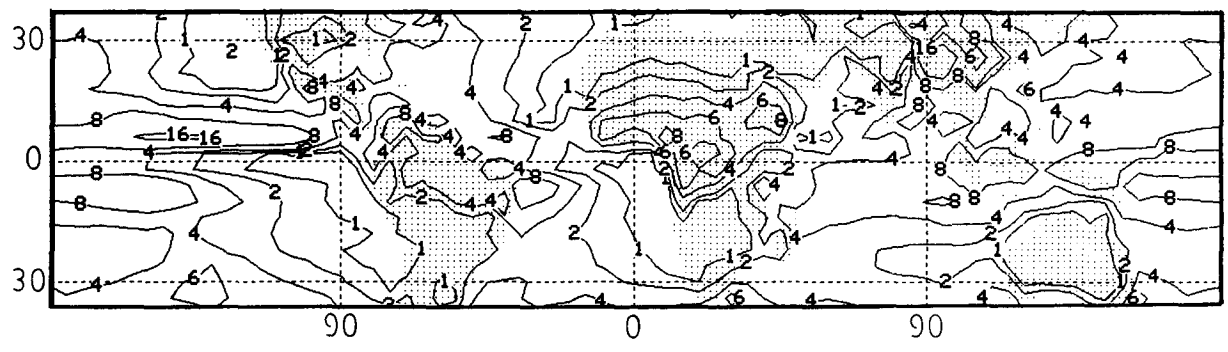

FIG. 6. Mean June–August modeled precipitation rate: control based on climatological SST (units: mm day^{-1}).

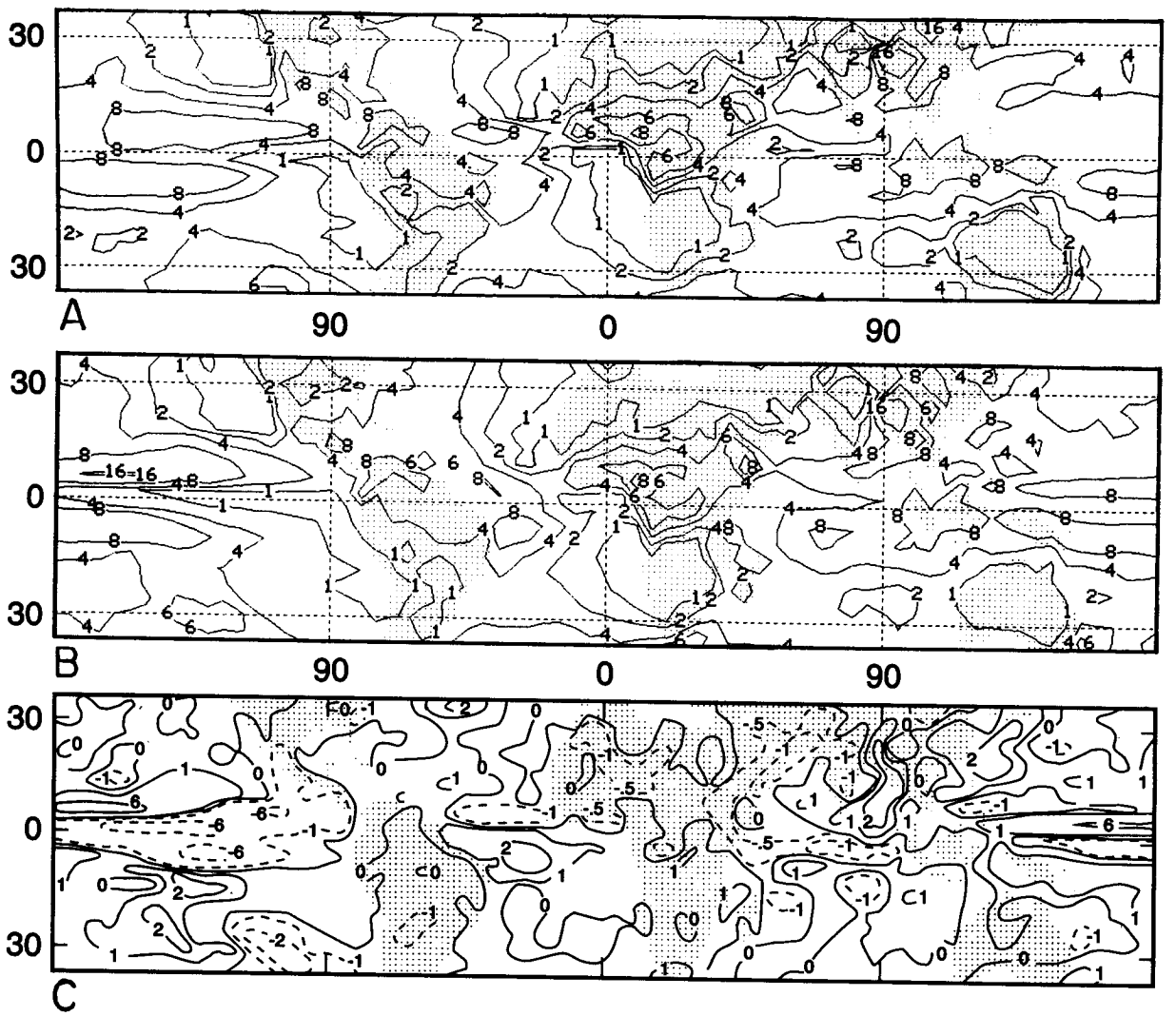

FIG. 7. Modeled June–August precipitation rate: (a) ENS87, (b) ENS88, and (c) ENS88 minus ENS87 (units: mm day^{-1}).

to the north is underestimated. Farther east, the Indian peninsula is too dry and the northern Bay of Bengal is perhaps too rainy. Over the central Pacific Ocean, the ITCZ maximum is well placed along 6°N, although there is excessive precipitation in this band and along 6°–10°S, compared with estimates by Shea (1986). June–August 13-year means (1971–83) of satellite-observed highly reflective clouds (HRC) show maxima of 5–6 days along 5°–7°N over the central Pacific (Garcia 1985), verifying the modeled position of the ITCZ and Shea's (1986) depiction. However, the 1971–83 mean HRC does not exceed 3 days anywhere over the Pacific southeast of 0°,180°. Moreover, HRC averages one or fewer days per month southeast of 0°, 160°W. This is additional evidence that the model tends to generate too much moist convection along 6°S, 180°–120°W, conceivably as a result of excessive moisture convergence in the lower troposphere. These unrealistic features of the modeled precipitation rate have an adverse effect on the model's sensitivity to 1988 minus 1987 SST differences.

Simulated precipitation rates for June–August are shown for ENS87 and ENS88 in Figs. 7a and 7b. With respect to tropical rainfall rates, ENS88 more closely resembles the control, while ENS87 exhibits various departures from both. The ENS88 minus ENS87 rainfall differences, shown in Fig. 7c, are most pronounced over the equatorial Pacific. Negative differences are evident between 2°S and 2°N, and over an even wider swath in the eastern Pacific. This area of ENS88 precipitation deficit coincides with the core of negative 1988 minus 1987 SST differences (Fig. 1c) and reflects the suppression of local moist convection over anomalously cold water in 1988 and the enhancement of convective rainfall over the warm 1987 SST (Arkin 1992). In contrast, positive rainfall differences along

6°N, (130°E–150°W) indicate a more northerly ITCZ in 1988. This simulated pattern of the 1988 minus 1987 precipitation differences is supported by OLR and HRC observations (Figs. 4 and 5), which both imply less convective activity along the equator in 1988 concomitant with greater activity along 10°N. Estimates of tropical rainfall rates derived from infrared satellite-based measurements for the same seasons (Janowiak and Arkin 1991) are consistent with this analysis.

Small negative ENS88 minus ENS87 precipitation differences over the Sahel and India are opposite in sign to observed 1988 minus 1987 differences from station data (Mo 1992) and to the positive differences in HRC frequency (Fig. 5c).

6. Discussion and conclusions

Simulations with the 4° × 5° resolution GISS GCM forced by SST of 1987 and 1988 for the contrasting June–August monsoon seasons reflect some of the observed differences in the general circulation. In particular, differences of 1988 versus 1987 in the 200-mb velocity potential reflect the observed dipole pattern of stronger, westward-displaced divergence over the Indian Ocean, along with stronger convergence over the South Atlantic to eastern South Pacific. Moreover, the simulated 1988 minus 1987 differences (ENS88 minus ENS87) in the 200-mb streamfunction show the distinctive cyclonic gyre over the tropical South Pacific, indicative of the stronger Walker circulation and weaker SWJ observed during the 1988 cold phase of an ENSO event. These streamfunction differences also imply a slightly stronger TEJ in 1988 over northern Africa and the North Indian Ocean, in qualitative agreement with observations.

The ENS88 minus ENS87 precipitation differences over the Pacific Ocean between 0° and 15°N are consistent with OLR and HRC evidence, which indicates a more northerly ITCZ in 1988. However, the modeled rainfall is too generous around 6°S and the simulated 1988 minus 1987 differences over the Sahel and India are opposite in sign to those observed.

Palmer et al. (1992) suggest that much of the interannual variation in Indian and Sahel precipitation can be accounted for by the remote effect of tropical Pacific SST anomalies acting through teleconnections in the planetary-scale circulation. Accordingly, limitations in the modeling of teleconnections between the strong Pacific SST forcing and the Asian–African monsoon appear relevant to the poor model representation of 1988 minus 1987 differences in monsoon rainfall.

ENS88 reflects the model bias for excess precipitation in June–August over the eastern tropical Pacific along 6°S, with rather large rates as far east as 130°W. Indeed, the OLR and HRC distributions for June–August 1988 (Figs. 4b and 5b) show little evidence for significant convective activity over the Pacific Ocean southeast of 0°,180°.

Local effects of the 1987 ENSO warm phase SST anomalies are apparent from the ENS87 precipitation pattern, which shows large values along 6°S from 150°E all the way to 120°W, as well as abundant rainfall along the equator. Significant convective activity in July over the southeast quadrant of the tropical Pacific is indeed more common during ENSO warm phases (Garcia 1985), and the OLR and HRC observations for June–August 1987 (Figs. 2a, 3a) confirm such activity between 5°–10°S, N 180°–165°W. Although the zonal extent of modeled precipitation southeast of 0°,180° is somewhat exaggerated in both simulations, the ENS87 distribution of rainfall is perhaps more realistic over the tropical Pacific than the corresponding ENS88 results.

We surmise that the model's systematic bias of exaggerating the precipitation rate along 6°S over the eastern Pacific narrows the zonal dimension of the Pacific Walker cell, especially in the simulation representing 1988 conditions. The moisture convergence and upward motion associated with this activity produces considerable divergence aloft which, in turn, distorts the eastern periphery of the upper-tropospheric outflow centered over Southeast Asia (Fig. 2e). This eastward stretching of the outflow region makes the upward portion of the zonal circulation cell too diffuse, weakening convection over South Asia, as well as the strength of the tropical easterly jet. The inadequate intensity of the Asian high-level divergence based on 1988 SST, in turn, fails to generate the observed excesses in 1988 rainfall (relative to 1987) over India and the Sahel. The relative weakness of the modeled ENS88 circulation over northern Africa has a similar origin since the eastward displacement of the 200-mb velocity potential minimum weakens the gradient of the isopleths west of India (Fig. 2e). Indeed, many of these features have been improved in more recent simulations with a newer version of the GCM that includes more realistic boundary layer and moist convection schemes.

These experiments explore the role of SST forcing in the general circulation over the Tropics. The local response of modeled precipitation to the extremely contrasting SST of 1987 and 1988 in the tropical Pacific Ocean; namely, the northward displacement of the eastern Pacific ITCZ from 1987 to 1988, is shown to be consistent with satellite observations. Discrepancies in the GCM simulation of June–August 1988 minus 1987 African–Asian monsoon rainfall differences appear to be related to model biases that distort particular features of the circulation that act as teleconnections between the Pacific and the Indian Ocean Basin. On the whole, however, the model offers reasonably realistic depictions of the upper-tropospheric irrotational and nondivergent wind fields and their 1988 minus 1987 differences. The study thus demonstrates a causal relationship between contrasting SST patterns and large

interannual differences in the tropical general circulation.

Acknowledgments. This study was supported by DOE Grant DE-FG02-92ER61477 and the NASA Climate Program (LD), and by NSF Grant ATM-9101097 and NOAA Grant NA26GP0088-01 (SH). The authors gratefully acknowledge the help of M. Fennessy, who provided NMC initial atmospheric conditions and SST data for the simulations, and D. Polzin in preparing HRC and OLR graphics.

REFERENCES

Arkin, P. A., 1992: Circulation and precipitation during the 1987 and 1988 monsoons. Simulation of interannual and intraseasonal monsoon variability. World Meteorological Organization TD-470, 2.1–2.6.

Del Genio, A., and M. Yao, 1993: Efficient cumulus parameterization for long-term climate studies: The GISS scheme. *The Representation of Cumulus Convection in Numerical Models, Meteor. Monogr.*, No. 46, K. Emanuel and D. Raymond, Eds., Amer. Meteor. Soc., 181–192.

Garcia, O., 1985: *Atlas of Highly Reflective Clouds for the Global Tropics: 1971–1983.* U.S. Dept. of Commerce, NOAA ERL, Boulder, 365 pp.

Hansen, J., G. Russell, D. Rind, P. Stone, A. Lacis, S. Lebedeff, R. Ruedy, and L. Travis, 1983: Efficient three-dimensional global models for climate studies: Models I and II. *Mon. Wea. Rev.*, **111**, 609–662.

Janowiak, J. E., and P. A. Arkin, 1991: Rainfall variations in the tropics during 1986–1989, as estimated from observations of cloud-top temperature. *J. Geophys. Res.*, **96**, 3359–3373.

Krishnamurti, T. N., H. S. Bedi, and M. Subramaniam, 1989: The summer monsoon of 1987. *J. Climate*, **2**, 321–340.

——, ——, and ——, 1990: The summer monsoon of 1988. *Meteor. Atmos. Phys.*, **42**, 19–37.

Mo, K. C., 1992: Impact of SST anomalies on the skill of seasonal forecasts and northern summer monsoons. *J. Climate*, **5**, 1249–1266.

Palmer, T. N., C. Brankovic, P. Viterbo, and M. J. Miller, 1992: Modeling interannual variations of summer monsoons. *J. Climate*, **5**, 399–417.

Philander, S. G., 1990: *El Niño, La Niña and the Southern Oscillation.* Academic Press, 293 pp.

Reynolds, R. W., 1988: A real-time global SST analysis. *J. Climate*, **1**, 75–86.

Shea, D. J., 1986: *Climatological Atlas:* 1950–1979. National Center for Atmospheric Research, TN-269+STR, 153 pp.

World Meteorological Organization, 1992: Report of workshop, simulation of interannual and intraseasonal monsoon variability. World Meteorological Organization TD-470, 1.1–1.39.